Available online at www.sciencedirect.com
ScienceDirect
Journal of Power Sources 165 (2007) 819–832
JOURNAL OF POWER SOURCES
www.elsevier.com/locate/jpowsour

Power management and design optimization of fuel cell/battery hybrid vehicles

Min-Joong Kim *, Huei Peng [1]

Department of Mechanical Engineering, University of Michigan, Ann Arbor, MI 48109-2125, United States

Received 17 October 2006; received in revised form 11 December 2006; accepted 12 December 2006
Available online 28 December 2006

Abstract

Power management strategy is as significant as component sizing in achieving optimal fuel economy of a fuel cell hybrid vehicle (FCHV). We have formulated a combined power management/design optimization problem for the performance optimization of FCHVs. This includes subsystem-scaling models to predict the characteristics of components of different sizes. In addition, we designed a parameterizable and near-optimal controller for power management optimization. This controller, which is inspired by our stochastic dynamic programming results, can be included as design variables in system optimization problems. Simulation results demonstrate that combined optimization can efficiently provide excellent fuel economy.

Keywords: Fuel cell vehicle; Hybrid vehicle; Power management; Design optimization

1. Introduction

Power management strategy and component sizing affect vehicle performance and fuel economy considerably in hybrid vehicles because of the multiple power sources and differences in their characteristics. Furthermore, these two important factors are coupled—different selection of component sizing should come with different design of power management strategy. Therefore, to achieve maximum fuel economy for hybrid vehicles, optimal power management and component sizing should be determined as a combined package. Our research has formulated and solved a combined power management/design (i.e., control/plant) optimization problem of a fuel cell hybrid vehicle (FCHV).

Development of the power management strategy is one of the important tasks in developing hybrid vehicles and relatively many literatures can be found. Guezennec et al. [1] solved the supervisory control problem of a FCHV as a quasi-static optimization problem and found that hybridization can significantly improve the fuel economy of FCHVs. Rodatz et al. [2] used the equivalent consumption minimization strategy to determine an optimal power distribution for a fuel cell/supercapacitor hybrid vehicle. The concept of equivalent factors in hybrid electric vehicles has been described by Sciarretta et al. [3]. In the same research, they also compared their power management result to deterministic dynamic programming result, which can lead to a global optimality.

Combined optimization problem of power management and component sizing of hybrid vehicles is analogous to a combined control/plant optimization problem in control theory. Fathy et al. [4] classified strategies for combined plant/controller optimization into sequential, iterative, bi-level, and simultaneous strategies. If a plant is optimized first and a controller is then designed, it often leads to non-optimal overall system due to the coupling of plant/controller optimization. Developing scalable subsystem models is essential in this optimization problem. Assanis et al. [5] proposed a design optimization framework to find the best overall engine size, battery pack, and motor combination in maximizing the fuel economy. For the engine scaling, in particular, they replaced the linear scaling of experimental engine lookup tables with a high-fidelity simulation that predicts the nonlinear effects of scaling. Fellini et al. [6] presented an

Abbreviations: DC/DC, direct current to direct current converter; FCHV, fuel cell hybrid vehicle; FC-VESIM, fuel cell hybrid vehicle simulation model; PEM, proton exchange membrane; PWM, pulse width modulator; SDP, stochastic dynamic programming; SOC, state of charge

* Corresponding author. Tel.: +1 734 936 0352; fax: +1 734 764 4256.
E-mail address: minjoong@umich.edu (M.-J. Kim).
[1] Tel.: +1 734 936 0352.

0378-7753/$ – see front matter © 2007 Elsevier B.V. All rights reserved.
doi:10.1016/j.jpowsour.2006.12.038

Nomenclature

C	capacity of battery
d	diameter
F	Faraday's number
I	current (A)
k	motor parameter
m	mass (kg)
M	molecular mass (kg mol^{-1})
n_{fc}	number of fuel cells
p	pressure (Pa) or probability
P	power (W)
R	gas constant or resistance (Ω)
T	temperature (K)
u	control input
v	longitudinal speed (m s^{-1})
V	voltage (V)
Vol	volume (m^3)
w	random parameter
W	mass flow rate (kg s^{-1})
x	design variable
y	mole fraction

Greek letters

Φ	non-dimensional compressor diameter
α	sensitivity slope in controller
ϕ	relative humidity
γ	air specific heat ratio or discount factor
η	efficiency
λ	excess ratio
ρ	density (kg m^3)
τ	torque (N m)
ω	rotational speed (rad s^{-1})
ψ	humidity ratio

Subscripts

a	air
amb	ambient
an	anode
aux	auxiliary
batt	battery
ca	cathode
cm	compressor motor
cp	compressor
cr	corrected
dcdc	DC/DC converter
fc	fuel cell
hm	humidifier
in	inlet
m	traction motor
out	outlet
oc	open circuit
rct	reacted
req	requested
sat	saturation
sm	supply manifold
st	fuel cell stack
t	terminal
v	vapor
veh	vehicle
wh	wheel

optimization algorithm of this problem. Their research provides a good framework for component sizing, but the control optimization was not addressed. Design optimization of FCHVs in the literature focused mostly on the relative size between battery and fuel cell (sometimes referred as the degree of hybridization). Ishikawa et al. of Toyota Motor Coporation [7] studied the effect of size ratios using their FCHV, but did not explain their control strategy and optimization procedure. Atwood et al. [8] used ADVISOR, developed by NREL, to study the degree of hybridization of a FCHV. They changed the ratio of the fuel cell over a fixed total power of powertrain and checked how the fuel efficiency varied. In a following paper [9], they included control variables in their optimization problem formulation. This was one of the earliest publications dealing with sequential control/plant optimization problem of FCHVs despite that the controller could not guarantee optimality. Another reference was published from Argonne National Laboratory [10], with an approach similar to [9]. In addition to component sizing optimization, Markel et al. [11] summarized design issues such as cost and volume in choosing types and sizes of the energy storage system for FCHVs.

Research in the optimization of hybrid vehicles was predominately conducted independently for either component sizing or control strategy; in rare cases when the two were considered together, control strategies were largely based on heuristic rules, which is usually far from true-optimality. This study presents a combined power management/design optimization of FCHVs. The power management algorithm was developed from stochastic dynamic programming motivated basis functions. In other words, while the control is not truly optimal, it is optimal in its sub-class. The overall problem is then recast into an optimal parameter problem.

2. Fuel cell vehicle model and optimal power management strategy

To study the combined power management/design optimization problem, we used the fuel cell hybrid vehicle simulation model (FC-VESIM), which was constructed based on the test data of a DaimlerChrysler prototype fuel cell vehicle *Natrium* [12]. The powertrain of *Natrium* consists of an 82 kW peak electric drive system, a 40 kW Li-ion battery pack and a 75 kW fuel cell engine. The prototype vehicle was tested in various conditions to verify its performances in highway driving, city driving, rapid acceleration, and maximum travel range while experimental data are collected from the vehicle components. During the several tests on proving ground, more than 200 channels of data were collected and used to build the simulation model. In

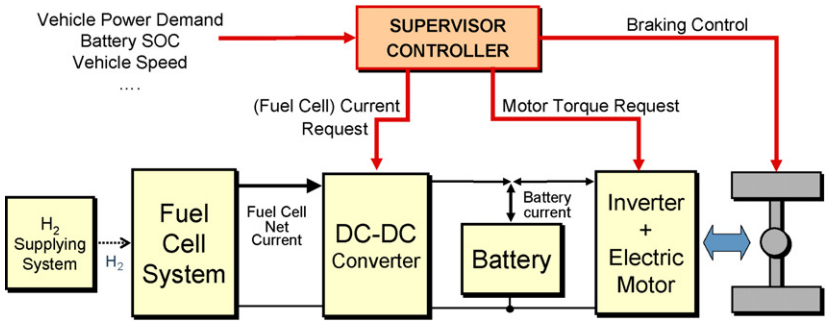

Fig. 1. Control signal flow in FC-VESIM. The power split ratio between the battery and the fuel cell system is managed by the supervisor controller sending the fuel cell net current request to the DC–DC converter.

addition to the vehicle, a fuel cell hybrid powertrain test bench was built. Each subsystem was tested on the bench to obtain necessary data to build its dynamic model and efficiency map.

Fig. 1 shows the powertrain schematic of FC-VESIM and key control signals for power management. FC-VESIM consists of several subsystems: driver, fuel cell system, battery, DC–DC converter, electric drive, and vehicle dynamics. Considering various vehicle states – such as power demand, battery state of charge (SOC), and vehicle speed – the supervisor controller sends the fuel cell current request to the DC–DC converter; sends the motor torque request to the electric drive; controls the regenerative braking ratio. In order to generate the motor torque requested from the supervisor controller, the inverter draws current from the electric DC bus where the battery and the DC–DC converter are connected in parallel. The DC–DC converter can control the current flow into the DC bus, whereas the battery here is "passively" connected to the DC bus—the difference between the current draw from the inverter and the current outflow from the DC–DC converter will be compensated by the passive battery. Therefore, the power split ratio between the battery and the fuel cell system is achieved by the supervisor controller sending the fuel cell net current request to the DC–DC converter.

The next step is to design subsystem-scaling models necessary to predict the respective characteristics of different sized components. The subsystem-scaling models we built can generate subsystem characteristics for each iteration of the optimization process. These characteristics can then be used in the simplified FC-VESIM.

The goal of power management in fuel cell hybrid vehicles is to minimize fuel consumption while maintaining the battery SOC by sending adequate current request command to the DC–DC converter. To achieve this goal, optimal power management strategy needs to be designed for the supervisor controller to balance the fuel cell system (FCS) power and the battery power. Many power management algorithms in technical literatures were designed by rule-based or heuristic methods. Those rule-based methods are simple and easy to understand because they come from engineering intuition. However, they often lack optimality or cycle-beating. Ideally, minimization of fuel consumption of hybrid vehicles can be achieved only when the driving scenario is known a priori. The deterministic dynamic programming technique can accomplish this global optimum. Then again, the result cannot be realized as a power management scheme because it is not possible to predict the future driving scenario.

The power management strategy designed by the stochastic dynamic programming (SDP) approach can overcome these limitations of existing algorithms [12]. The idea of the infinite horizon SDP is that if the overall power demand is modeled as a stochastic process, an optimal controller can be designed based on the stochastic model. First, the driver power demand is modeled as a discrete-time stochastic dynamic process by using a Markov chain model, which is constructed from standard driving cycles. In other words, the power demand from the drive at the next time step depends on the current power demand and vehicle speed:

$$p_{il,j} = \Pr\{w = P^j_{\text{dem}} | P_{\text{dem}} = P^i_{\text{dem}}, \omega_{\text{wh}} = \omega^l_{\text{wh}}\},$$
$$\text{for } i, j = 1, 2, \ldots, N_p, \quad l = 1, 2, \ldots, N_\omega \tag{1}$$

where the power demand P_{dem} and the wheel speed ω_{wh} are quantized into grids of N_p and $N_{\omega,}$ respectively. Then, for the discretized state vector, $x = (\text{SOC}, \omega_{\text{wh}}, P_{\text{dem}})$, corresponding optimal fuel cell current request command, $u = I_{\text{fc,net,reg}}$, is determined to minimize the expected cost of hydrogen consumption and battery energy usage over infinite horizon:

$$J = \lim_{N\to\infty} \underset{w_k}{E} \left\{ \sum_{k=0}^{N-1} \gamma^k (W_{\text{H}_2,\text{rct}} + W_{\text{soc}}) \right\} \tag{2}$$

where $0 < \gamma < 1$ is the discount factor, $W_{\text{H}_2,\text{rct}}$ the reacted hydrogen mass, and W_{soc} penalizes the battery energy use based on the SOC value. This SDP problem can be either solved by a policy iteration or value iteration process. The resulting SDP control strategy generates optimal fuel cell current request as a function of battery SOC, wheel speed, and power demand. The control strategy achieves high fuel economy while successfully maintaining battery SOC.

Despite the advantages of the SDP approach, it is computationally expensive to build tables and get a corresponding optimal control for complex dynamic systems. Moreover, component design variables cannot be included in a standard SDP problem formulation. The iterative algorithms solving SDP problems need a cost table and a transition probability table, but those tables can be constructed only by a vehicle model with fixed component sizes—if we want to change component sizes in optimization process, we end up getting double loop of time

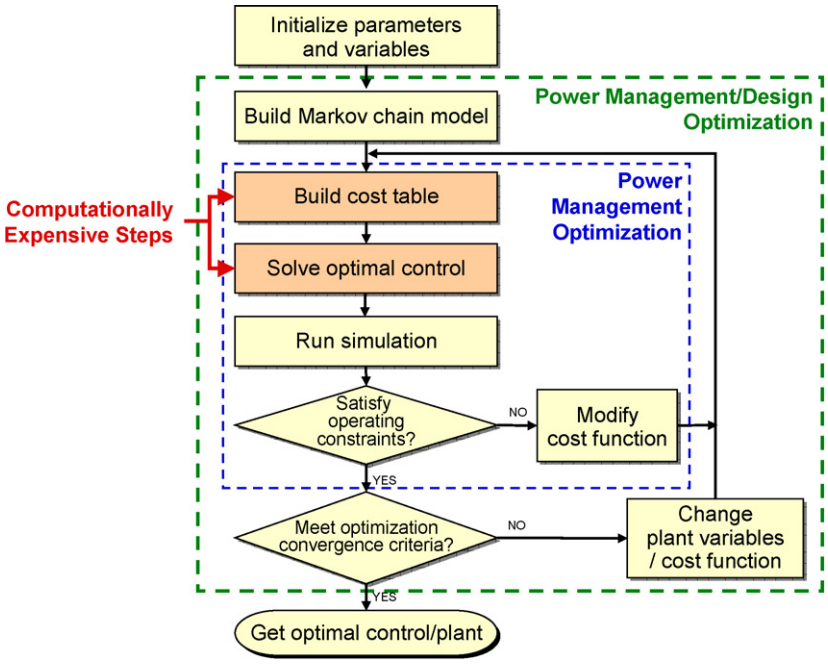

Fig. 2. Flowchart of combined power management/design optimization problem if SDP process is applied. Double loops of computationally expensive steps in the SDP make this process infeasible.

consuming iteration process (Fig. 2). This makes iterations for different system designs even more difficult. These limitations of the SDP approach, therefore, make it unsuitable for combined power management/design optimization problems.

To overcome these limitations of the SDP approach, we developed a near-optimal controller for optimization process. This controller has an advantage over the SDP—it can be included as several design variables in the standard optimization process because it is parameterized. On the other hand, because of its similarity to the SDP result, the controller has advantage over heuristic methods in that it is near-optimal.

3. Optimization Problem Formulation

This section describes how the combined power management/design optimization problem was formulated. Section 3.1 explains how the fuel cell system and the battery are scaled, and how the concept of degree of hybridization places restriction on the amount of active materials in fuel cells and battery. In Section 3.2, the optimal controller result based on the stochastic dynamic programming is parameterized, so that the power management strategy can be included as design variables in the optimization process. The final form of problem statement is made in Section 3.3.

3.1. Subsystem-scaling models of fuel cell hybrid powertrain

Although linear scaling is appropriate for predicting system characteristics when size deviations from the baseline design are small, it becomes less accurate when the deviations are large, especially for highly nonlinear systems. Therefore, we found it necessary to develop subsystem-scaling models for fuel cell hybrid powertrains that could predict the sizing effects of components including the number of fuel cells, compressor diameter and battery capacity.

3.1.1. Fuel cell system-scaling model

We developed a static FCS scaling model to predict how the design variables – number of fuel cells and compressor diameter scale – affect the efficiency characteristics of the fuel cell system. The fuel cell system consists of the fuel cell stack, which is a serially layered pack of fuel cells, and the system auxiliary components, which include compressor, cooling/heating devices, and water management systems. For the fuel cell stack, because change in the active cell area requires the complete redesign of flow channels, we chose the number of fuel cells as a design variable. Among the auxiliary components, we chose the compressor diameter scale as a design variable because the compressor power is the biggest draw on fuel cell auxiliary powers.

Since the fuel cell system is the primary power source of fuel cell hybrid vehicles, the fuel cell stack is the core of the powertrain—it is comparable to the cylinders of the combustion engine. Possible design changes of the fuel cell stack are the number of fuel cells and the active cell area. By changing them, we can obtain different characteristics of the fuel cell stack current and voltage relation. To build the current–voltage relation model, we collected data from the fuel cell system on a test bench [12], did the curve-fitting, and obtained the polarization curve, which is shown in Fig. 3. Here, we assumed that the temperature is maintained at the operating condition (around 75–80 °C) and ignored the effect of the pressure difference between the cathode and the anode. As a result, the cell voltage (V_{cell}) is denoted by the current density (i_{st}) and the system pressure (p_{sys}): $V_{cell} = f(i_{st}, p_{sys})$. We used this equation as the reference of

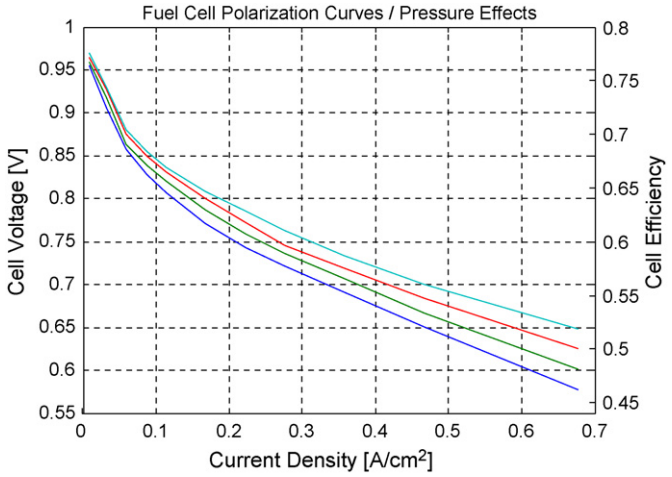

Fig. 3. Fuel cell polarization curve with respect to different levels of cathode pressure. Changes in the fuel cell stack design do not affect this curve since it is the property of the cell.

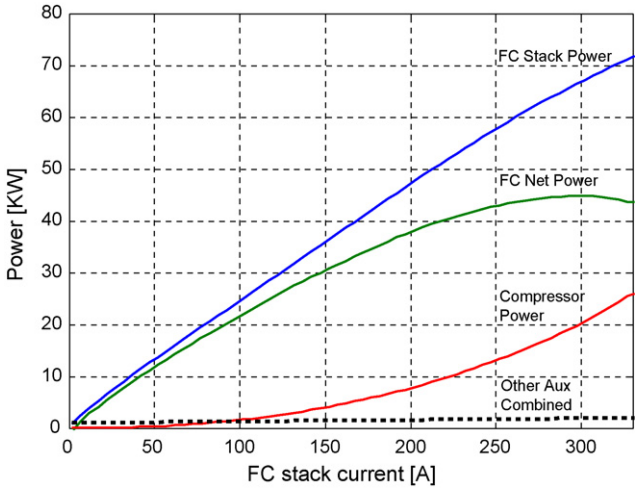

Fig. 4. Comparison of fuel cell stack power, net power, and auxiliary power vs. fuel cell stack current. The compressor auxiliary power is most influential determining the fuel cell net power and fuel cell system efficiency because it dominates the fuel cell auxiliary power.

fuel cell stack scaling because the polarization curve is the property of the fuel cell, which is largely unaffected by cell numbers of a stack. Theoretically, if the number of fuel cells is changed, multiplication of the single cell voltage of the polarization curve will be the stack voltage because the cells are serially connected. It is also easy to change the number of fuel cells because fuel cell units can be stacked up without much difficulties. On the other hand, if the fuel cell active area is changed, we should get the x-axis scaled because the unit of the x-axis is the current density ($\mathrm{A\,cm^{-2}}$). However, in practice, it is not simple to modify the active cell area because it requires re-design of the reactant flow channel, which is a complicated and time-consuming process. Moreover, the re-design of the reactant flow channel can influence the humidity and thermal characteristics of the stack, and consequently it may not be guaranteed that the same polarization curve can be used for the scaled design. Therefore, for practical design purpose, only the number of fuel cells (n_{fc}) is chosen as a design variable for the fuel cell stack in this study.

Among the fuel cell auxiliary components, the compressor draws our most attention in terms of system efficiency, because the compressor is the most energy-consuming component. From our data shown in Fig. 4, the compressor power can be up to 30% of the fuel cell system stack power, whereas power consumption by other auxiliary components is relatively not as significant as that of the compressor. Similar observation was reported by Boettner et al. [13], where the compressor power is up to 93.5% of the total auxiliary power consumption. Therefore, we chose the compressor diameter scale as a design variable because the compressor is the major draw on auxiliary power. We scaled power consumption of other auxiliaries proportional to the ratio of the number of fuel cell to that of the baseline design.

We developed a static FCS model based on our test data and the model parameters of the previous study [14]. To reduce the computational time of the optimization process, the FCS scaling model eventually will generate simple static maps, which relate the fuel cell net current to the fuel cell stack voltage, auxiliary power, and hydrogen fuel consumption. The static FCS scaling model takes the stack current as the system input. Since the stack current determines the amount of reacted oxygen, we can calculate the required amount of air inflow to the cathode by assuming constant excess ratio and mass fraction of the oxygen. In reality, before we draw net current from the fuel cell system and the internal controller starts to drive the compressor motor, we cannot estimate the fuel cell stack current in advance. However, since there is no dynamics involved in this scaling model, causality is not an issue because all the input–output relations are stationary one-to-one correspondences.

Fig. 5 illustrates the air supplying system for the fuel cell cathode. No sizing issue is involved in the anode side because a pressurized tank and a control valve are typically used to supply hydrogen fuel. In this scaling model, therefore, only the air supplying subsystem will be considered. For a given stack current, the inlet air to the cathode is calculated by assuming constant mass fraction of the oxygen inside the cathode:

$$W_{\mathrm{O_2,rct}} = \frac{n_{\mathrm{fc}} M_{\mathrm{O_2}} I_{\mathrm{st}}}{4F},$$
$$W_{\mathrm{a,ca,in}} = \frac{\lambda_{\mathrm{O_2}} W_{\mathrm{O_2,rct}}}{y_{\mathrm{O_2,ca}}} = \frac{\lambda_{\mathrm{O_2}} n_{\mathrm{fc}} M_{\mathrm{O_2}} I_{\mathrm{st}}}{4 y_{\mathrm{O_2}} F} \tag{3}$$

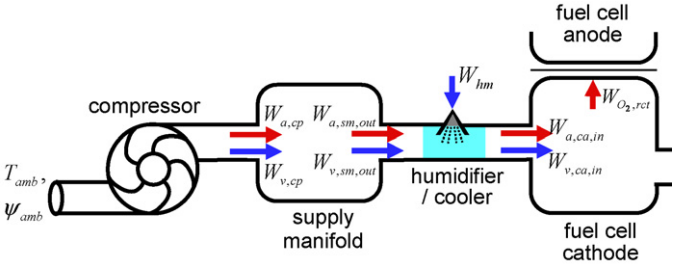

Fig. 5. Air supplying subsystem of the fuel cell system. Static compressor model determines the amount of the air supply by the compressor from the amount of oxygen reacted in the fuel cell cathode.

where F is the Faraday number, n_{fc} the number of fuel cells, M_{O_2} the molar mass of oxygen, and λ_{O_2} is the oxygen excess ratio which is assumed to be maintained at a desired level ($\lambda_{O_2} = 2$). By the conservation of mass, the dry air mass flow at the cathode inlet, supply manifold outlet, and the compressor outlet are identical at the steady state ($W_{a,ac,in} = W_{a,sm,out} = W_{a,cap}$), and the water vapor mass flow at the supply manifold outlet and the compressor outlet is the same as well ($W_{v,sm,out} = W_{v,cp}$). The humidifier provides the water vapor W_{hm} to the inlet air such that the relative humidity in the cathode is 100% at 80 °C. With these assumptions, the compressor outlet flow is calculated from:

$$W_{cp} = W_{a,cp} + W_{v,cp} = (1 + \psi_{amb})W_{a,cp} = \left(1 + \frac{M_v \phi_{amb} p_{sat,amb}}{M_a p_{a,amb}}\right) W_{a,ca,in} = \left(1 + \frac{M_v \phi_{amb} p_{sat,amb}}{M_a p_{a,amb}}\right) \frac{\lambda_{O_2} n_{fc} M_{O_2} I_{st}}{4 y_{O_2} F}, \quad (4)$$

where ψ_{amb} is the humidity ratio of the atmospheric air, M_a and M_v the dry air molar mass and vapor molar mass, respectively, ϕ_{amb} the relative humidity of the ambient air (assumed to be 0.5), $p_{sat,amb}$ the vapor saturation pressure at ambient temperature, and $p_{a,amb}$ is the pressure of the dry atmospheric air.

The key of fuel cell system-scaling model lies in the compressor model. In this scaling model, the compressor is assumed to operate following a steady-state operating trajectory on the compressor map as shown in Fig. 6. This compressor model is non-causal in that the pressure ratio and the compressor speed are obtained backwards from the given flow rate. The figure also suggests that there exists a minimum air flow rate to avoid compressor surging. The compressor torque is derived by using the thermodynamic equation:

$$\tau_{cp} = \frac{C_p}{\omega_{cp}} \frac{T_{amb}}{\eta_{cp}} \left[\left(\frac{p_{sm}}{p_{amb}} \right)^{(\gamma-1)/\gamma} - 1 \right] W_{cp}, \quad (5)$$

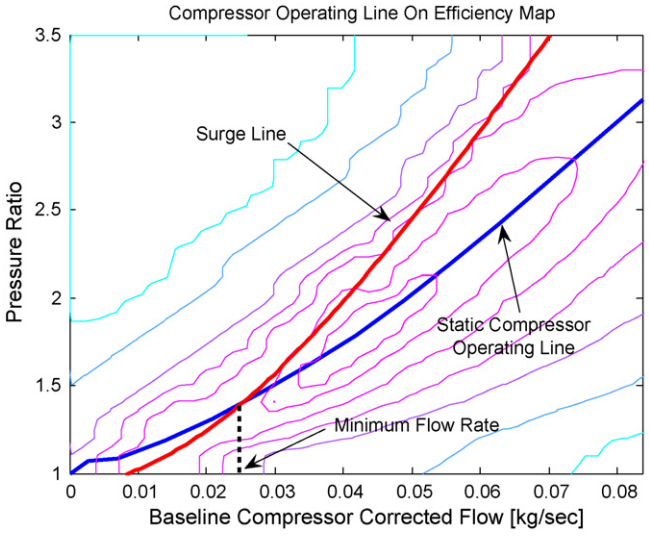

Fig. 6. Compressor operating line on efficiency map. The compressor is operated following a static operating line, and minimum flow rate is determined to prevent compressor surging phenomenon.

where the compressor efficiency η_{cp} is given from the efficiency map, and the compressor speed ω_{cp} and pressure ratio (p_{sm}/p_{amb}) can be obtained by assuming a static operating compressor. The compressor power consumption can then be calculated,

$$P_{cm} = V_{cm} I_{cm} = V_{cm} \frac{\tau_{cp}}{\eta_{cm} k_t}, \quad (6)$$

where η_{cm} is the compressor motor efficiency and k_t is the motor constant. After getting the compressor power consumption, it is subtracted from the FC stack power to obtain the FC net power and net current:

$$I_{net} = \frac{P_{st} - (P_{cm} + P_{aux})}{V_{st}} = I_{st} - \frac{P_{cm} + P_{aux}}{V_{st}}, \quad (7)$$

where other auxiliary power consumption P_{aux} is linearly scaled by the number of fuel cells from the baseline FCS. In addition, from the stack current we can calculate the hydrogen fuel consumption:

$$W_{H_2,rct} = \frac{n_{fc} M_{H_2} I_{st}}{2F} \quad (8)$$

By repeating this procedure for different FC stack current levels, we can obtain simple static maps, which relate the FC stack current to the FC net current, the FC stack voltage, and the hydrogen fuel consumption. Since all these relations are stationary one-to-one correspondences, we can take the FC net current as the input of these static maps, so that they can be used in the two-state FC-VESIM model for iteration.

The compressor sizing effect is nonlinear due to its dynamic and nonlinear characteristics of compressor map and efficiency. As explained above, the compressor dynamics is ignored by using the static operating trajectory in Fig. 6. For the compressor scaling, it is assumed that the normalized compressor flow rate Φ is constant for a specific compressor design regardless of its diameter scale, and that the range of the pressure ratio does not change. The normalized compressor flow rate can be expressed [15] as:

$$\Phi = \frac{W_{cr}}{\pi/4 \rho_a d_{cp}^2 U_{cp}}, \qquad U_{cp} = \omega_{cp} \frac{d_{cp}}{2}, \quad (9)$$

where W_{cr}, ρ_a, d_{cp} are the corrected compressor flow, the air density, and the compressor diameter, respectively. U_{cp} is the compressor blade tip speed, which is proportional to the compressor speed ω_{cp}. Consequently, Eq. (9) becomes:

$$\Phi = \frac{W_{cr}}{\pi/8 \rho_a d_{cp}^3 \omega_{cp}}. \quad (10)$$

Since we assumed a constant normalized flow rate Φ, the following relation is obtained:

$$\frac{W_{cr,scaled}}{W_{cr,baseline}} = \left(\frac{d_{cp,scaled}}{d_{cp,baseline}} \right)^3 = x_{cp}^3, \quad (11)$$

where x_{cp} denotes the compressor diameter scale. As a result, it is possible to obtain a new flow rate map of the scaled compressor by scaling the x-axis, i.e., the corrected flow indexes of the baseline compressor flow map by x_{cp}^3. This approach can be applied to scale the compressor efficiency map as well.

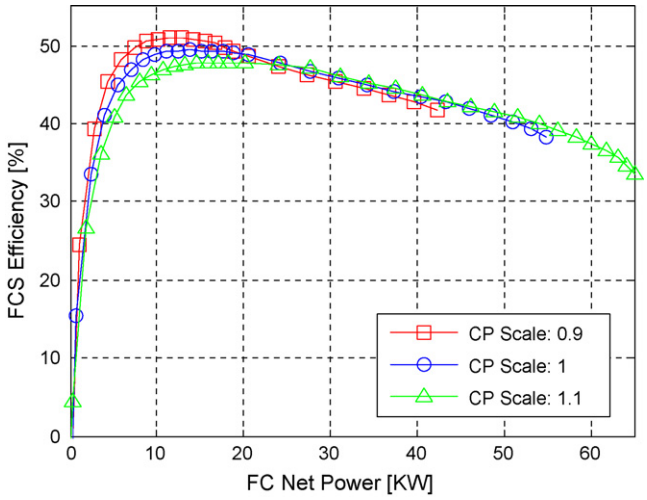

Fig. 7. Compressor size effect on fuel cell system efficiency. As the compressor diameter increases, maximum fuel cell net power is increased while the system efficiency is decreased especially in the low power region.

Fig. 7 shows the compressor diameter sizing effect on the system efficiency map when the number of fuel cells and other system parameters are fixed. The trade-off of compressor sizing is as follows: a fuel cell system with a smaller compressor has better efficiency in the low power range, however, the maximum fuel cell net power is decreased. On the other hand, a fuel cell system with a larger compressor loses efficiency in the lower power range, but it can achieve more maximum fuel cell net power. The maximum fuel cell net power is determined by the fuel cell net current, which is limited by the compressor size and characteristics:

$$I_{\mathrm{fc,net}}^{\max} = \min\left\{ I_{\mathrm{fc,net}} \,\middle|\, p_{\mathrm{ca}}(I_{\mathrm{fc,net}}) = p_{\mathrm{ca}}^{\max},\, I_{\mathrm{fc,net}} \middle|\, W_{\mathrm{cr}}(I_{\mathrm{fc,net}}) = W_{\mathrm{cr}}^{\max},\, I_{\mathrm{fc,net}} \middle| \frac{\Delta P_{\mathrm{fc,net}}}{\Delta I_{\mathrm{fc,net}}} < 0 \right\}, \tag{12}$$

where p_{ca}, W_{cr}, $P_{\mathrm{fc,net}}$ are the cathode pressure, the corrected compressor flow, and the fuel cell net power, respectively.

3.1.2. Battery scaling model

A propulsion battery system consists of serially connected battery cells. The battery system is relatively simple, compared to a fuel cell system, which has substantial number of auxiliary components and requires a controller to supply hydrogen and oxygen fuels.

A battery pack can be scaled simply according to its number of cells and the cell capacity, but we chose only the capacity as a design variable in this study. This allows us to sustain the nominal voltage of the inverter side. In the configuration of DaimlerChrysler Natrium FCHV (Fig. 1), the battery pack terminals are directly connected to the electric DC bus, so the battery terminal voltage becomes the electric DC bus voltage. This means that the inverter side voltage will change with the changes in the number of battery cells. Since the inverter voltage should be maintained in the operating range, it is undesirable to change the number of cells without an extra DC–DC converter for the battery side. The extra DC–DC converter will decrease the powertrain efficiency and lead to a complex control problem of the DC bus voltage and the battery SOC. We avoid these consequences by fixing the number of battery cells.

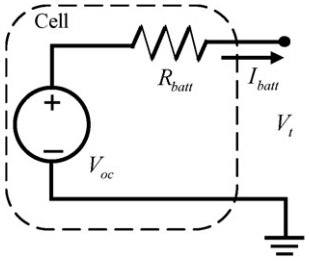

Fig. 8. One resistance battery model. It is simple and enables fast simulation for optimization process.

We developed a resistance battery model for scaling and optimization purposes using the SAFT lithium-ion battery test data (Fig. 8). The one-state battery model is an equivalent circuit model with a voltage source and an internal resistance (Fig. 2). The terminal voltage of the battery pack, V_{batt}, can be denoted by:

$$V_{\mathrm{batt}} = n_{\mathrm{batt}}(V_{\mathrm{oc}} - R_{\mathrm{batt}} I_{\mathrm{batt}}), \tag{13}$$

where n_{batt} is the number of battery cells; V_{oc} the open circuit voltage, which is a nonlinear function of battery SOC and temperature; R_{batt} is the battery internal resistance, which is a function of battery SOC, temperature, and the current direction (charge/discharge). Following the battery test profile [16], the open circuit voltage was measured and battery resistance was calculated for different levels of battery SOC. The battery temperature was assumed to be room temperature, i.e., 25 °C. The battery SOC is defined as:

$$\mathrm{SOC}(t) = \mathrm{SOC}_0 - \frac{1}{C_{\mathrm{batt}}} \int_{t_0}^{t} I_{\mathrm{batt}} \mathrm{d}t \tag{14}$$

where C_{batt} denotes the battery cell capacity and k is the time step.

The characteristics of a battery pack change as its battery capacity scale x_{battCap} changes:

$$x_{\mathrm{battCap}} = \frac{C_{\mathrm{batt,scaled}}}{C_{\mathrm{batt,baseline}}}. \tag{15}$$

Because the active material of the cells has the maximum current density limit and the battery cells are connected in series, the battery pack power and current limits are proportional to x_{battCap}, whereas the pack voltage limits remain the same. The scaled limits are:

$$\begin{aligned} \{P_{\mathrm{batt,scaled}}^{\max}, P_{\mathrm{batt,scaled}}^{\min}\} &= x_{\mathrm{battCap}}\{P_{\mathrm{batt,baseline}}^{\max}, P_{\mathrm{batt,baseline}}^{\min}\} \\ \{I_{\mathrm{batt,scaled}}^{\max}, I_{\mathrm{batt,scaled}}^{\min}\} &= x_{\mathrm{battCap}}\{I_{\mathrm{batt,baseline}}^{\max}, I_{\mathrm{batt,baseline}}^{\min}\} \end{aligned}, \tag{16}$$

where $P^{\max}$ and $P^{\min}$ are maximum discharging and charging power limits. The battery capacity scaling changes the battery pack resistance. For the same amount of discharging current, the cell current density decreases as x_{battCap} increases, thus the cell

voltage drop decreases. This is represented by the following:

$$\{R^{+}_{\text{batt,scaled}}, R^{-}_{\text{batt,scaled}}\} = \frac{1}{x_{\text{battCap}}}\{R^{+}_{\text{batt,baseline}}, R^{-}_{\text{batt,baseline}}\}, \tag{17}$$

where R^{+} and R^{-} denote discharging and charging resistance, respectively. The battery should work within its power, current, and voltage limits, which are

$$\{P^{\min}_{\text{batt}}, I^{\min}_{\text{batt}}, V^{\min}_{\text{batt}}\} < \{P_{\text{batt}}, I_{\text{batt}}, V_{\text{batt}}\} < \{P^{\max}_{\text{batt}}, P^{\max}_{\text{batt}}, P^{\max}_{\text{batt}}\} \tag{18}$$

3.1.3. Degree of hybridization

In a typical process of vehicle powertrain design, the maximum peak power to satisfy vehicle performance requirements (drivability) is determined first. For hybrid vehicles, the degree of hybridization (DOH) should then be determined. For hybrid electric vehicles, the DOH is the ratio of the combustion engine power to the total powertrain power, and for FCHVs, it would be the ratio of the FCS net power to the total powertrain power. In this study however, we need a different definition of DOH because the FCS net power depends not only on the FC stack size but also on the flow capacity of its compressor. Since fuel cells and battery cells are much more expensive than compressors, the DOH definition should focus on the active materials.

To define the DOH, we started from the baseline 60 kW fuel cell system with 381 cells and the baseline 60 kW Li-ion battery pack with 7.035 Ah. Since these two components have the same maximum power rate, their combination builds a 0.5 DOH fuel cell hybrid powertrain. Then, focusing on the active materials, the degree of hybridization is defined as follows:

$$\frac{n_{\text{fc,scaled}}}{n_{\text{fc,baseline}}} = \frac{x_{\text{DOH}}}{x_{\text{DOH,baseline}}},$$

$$\frac{C_{\text{batt,scaled}}}{C_{\text{batt,baseline}}} = \frac{1 - x_{\text{DOH}}}{1 - x_{\text{DOH,baseline}}},$$

$$\text{where } x_{\text{DOH,baseline}} = \frac{P^{\max}_{\text{fcNet,baseline}}}{P^{\max}_{\text{fcNet,baseline}} + P^{\max}_{\text{Batt,baseline}}}. \tag{19}$$

Note that one x_{DOH} value determines both n_{fc} and x_{battCap} at the same time. For example, if DOH is 0.6, the number of fuel cells increases by 20% (0.6/0.5 = 1.2) of the baseline number of cells ($n_{\text{fc,baseline}}$), while the battery capacity decreases by 20% (0.4/0.5 = 0.8) of the baseline capacity ($C_{\text{batt,baseline}}$). If DOH = 1, the powertrain becomes a "pure fuel cell vehicle" without battery, and if DOH = 0, then it becomes a "pure battery electric vehicle."

One of our optimization goals is to find an optimal "active material distribution" between 0 and 1 of DOH. If x_{DOH} increases, the number of fuel cells will increase. The FCS can take advantages of the higher voltage—for the same FC power demand, the FCS can be operated in a lower current region where the FCS efficiency is higher. The increase of x_{DOH}, however, results in a decrease of battery capacity. This may reduce the amount of regenerative braking energy due to the decreased power limits, and the battery may not be able to assist with enough power during rapid acceleration. Such a trade-off of DOH leads to the existence of bounded optimal solutions.

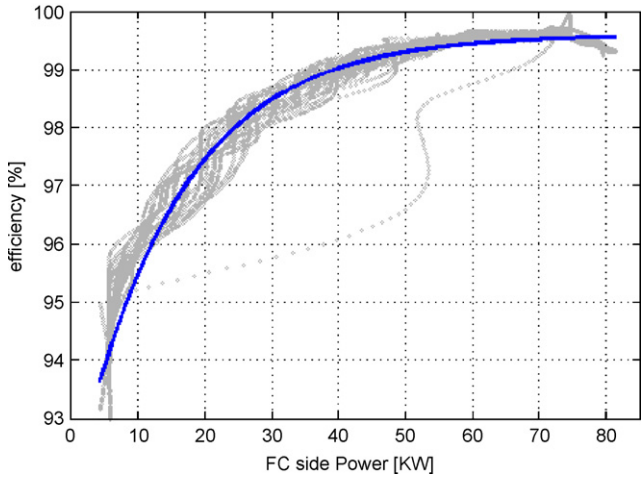

Fig. 9. DC/DC converter efficiency.

3.1.4. DC/DC converter and electric drive

Among the components of the fuel cell hybrid powertrain, major subsystems to be discussed are the DC/DC converter and the electric drive. We linearly scaled the DC/DC converter efficiency curve with respect to the number of fuel cells ratio to that of the baseline design. It means that the DC/DC converter size is a dependent variable to the fuel cell system size. This assumption is reasonable because the DC/DC converter is a device to transfer the fuel cell power to the DC bus, and it has relatively consistent and high efficiency, which ranges from 95 up to 99.5% with respect to the fuel cell side power (Fig. 9).

Meanwhile, we fixed the size of the electric drive. For optimization problems of hybrid electric vehicles, the electric motor size can be considered as a design variable [5]. Because hybrid electric vehicles use two propulsion sources—conventional engine transmission and electric motor, the split between the two can be an optimization problem. However, fuel cell hybrid vehicles use the electric motor as the only source of propulsion power. The motor size, therefore, should be determined at the early stage of vehicle powertrain design to satisfy the peak power requirements.

3.2. Power management controller—parameterized "pseudo-SDP controller"

In this study, we used "pseudo-SDP controller" for the combined power management/design optimization. The pseudo-SDP controller is a near-optimal controller inspired by the SDP control results. Unlike the original SDP controller, the pseudo-SDP controller uses basis functions observed from SDP control laws and can be represented with a few variables such that they can be used as optimization design variables. Unlike other heuristic rule-based algorithms, the pseudo-SDP controller generates near-optimal results because its topology (basis function) is from the optimal SDP controller. The combined power management/design optimization problem becomes a standard

nonlinear optimization problem with several design variables and constraints (Fig. 10).

In the stochastic dynamic programming, problem formulation starts from probability modeling of future power demand by observing standard driving cycles. The idea is to minimize the cost function over a class of trajectories from an underlying Markov chain driving cycle generator. Unlike deterministic dynamic programming (DDP), whose result is a set of control trajectories over the time horizon, the SDP produces a set of optimal controls for each state and can be implemented as a full-state feedback lookup table. Whereas changes in the vehicle power demand or the battery SOC directly influence the required FC power, the vehicle speed variable influences only the probability distribution of the future vehicle power demand. Therefore, the three-state optimal controller can be simplified by eliminating the vehicle speed state as in

$$I^*_{\mathrm{fc,req}} = f(\mathrm{SOC}, v_{\mathrm{veh}}, P_{\mathrm{dem}}) \approx f_1(\mathrm{SOC}, P_{\mathrm{dem}}). \quad (20)$$

The SDP controller consists of "layers" of vehicle speed levels. Our original design [12] used 15 levels of vehicle speeds ranging from 0 to 80 mph. Interestingly, as seen in Fig. 11, it was noted that contour shapes are very similar to each other with the exception of layers near zero. The 20 mph layer was used as a standard map in designing a near-optimal "pseudo-SDP controller."

At a fixed vehicle speed, the SDP controller is parameterized using four variables. Fig. 12 illustrates how the original contour

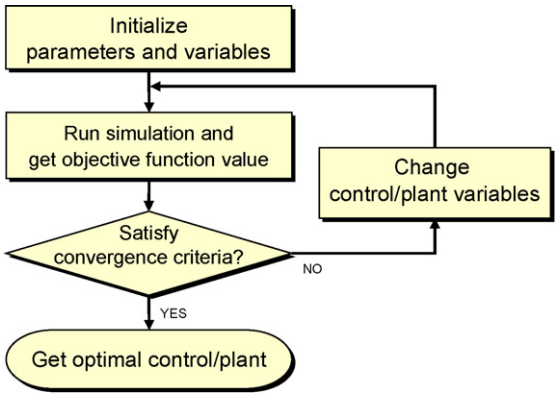

Fig. 10. Proposed optimization process using pseudo-SDP controller. Power management strategy and component sizes are represented as design variables in a standard form of nonlinear optimization process.

is simplified as a set of straight lines. The x and y-axes represent the battery SOC and vehicle power demand, respectively. As the battery SOC decreases—or the vehicle power demand increases, it is apparent that the optimal current request will increase. The maximum FC current density request ($x_{i\max}$), therefore, takes place at the intersection between the lower bound of the SOC and the upper bound of the vehicle power demand, i.e., the upper left corner of Fig. 12. The profile of the straight-lined contour is parameterized as an exponential curve with a constant (x_α) so that the current density command reaches exponentially from 0

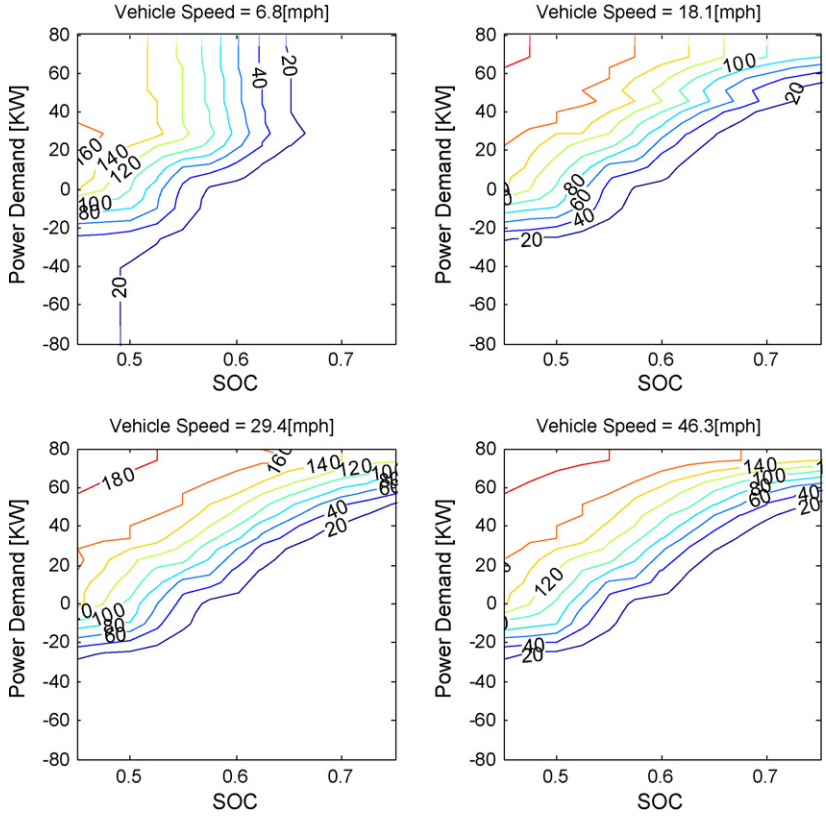

Fig. 11. Original SDP controller for vehicle speed levels of 6.8, 18.1, 29.4, and 40.7 mph. Unless the vehicle speed is near zero, the shape of control contour is very similar to each other regardless of vehicle speed levels.

to $x_{i\max}$:

$$i_{\text{req}} = \frac{1 - e^{-\sigma\xi}}{1 - e^{-\sigma}} i_{\max},$$

where i_{req} is the current density command and ξ is a normalized distance ranging from 0 to 1. The sensitivity slope (x_α) is another variable that affects the sensitivity of the control map to the unit changes in the battery SOC and vehicle power demand. x_α is also subject to change largely by the power ratio between the FCS and the battery pack, i.e., degree of hybridization. The unit of x_α is radian, based on the normalized SOC and vehicle power demand (both range from −1 to 1). Another variable that frames the pseudo-SDP controller is the battery SOC value when the vehicle power demand is zero ($x_{\text{stableSOC}}$). If an FCHV stops and its engine keeps idling, the battery will be charged until it reaches $x_{\text{stableSOC}}$. Therefore, it will be the initial battery SOC value of a starting vehicle. $x_{\text{stableSOC}}$ plays a significant role in managing the battery SOC because it is the target SOC value, to which the near-optimal controller tends to charge the battery back. As a result, the values of these four variables – $x_{i\max}$, x_σ, x_α, $x_{\text{stableSOC}}$ – can determine a unique pseudo-SDP controller.

Two extreme cases of the pseudo-SDP controller are shown in Fig. 13. If x_α is near zero, the FCS will mainly follow the vehicle power demand as in Fig. 13(a). If, on the other hand, x_α is near $\pi/2$, it will try to keep only the battery SOC. Moreover, as x_σ becomes large, the controller characteristics will be similar to those of an "On/Off" controller. Fig. 13(b) shows an example of an on/off type controller switched by the battery SOC level.

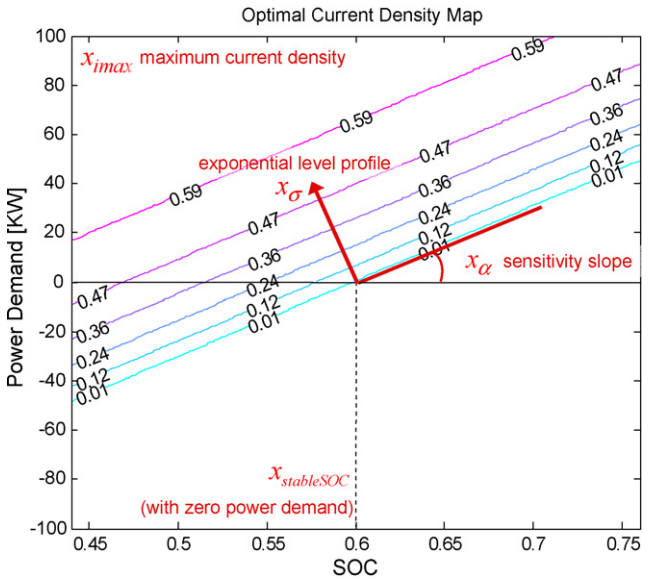

Fig. 12. Pseudo-SDP controller. Four design variables – x_α, x_σ, $x_{i\max}$, $x_{\text{stableSOC}}$ – uniquely determine one power management strategy.

The pseudo SDP controller allows us to easily satisfy subsystems constraints without compromising fuel economy compared

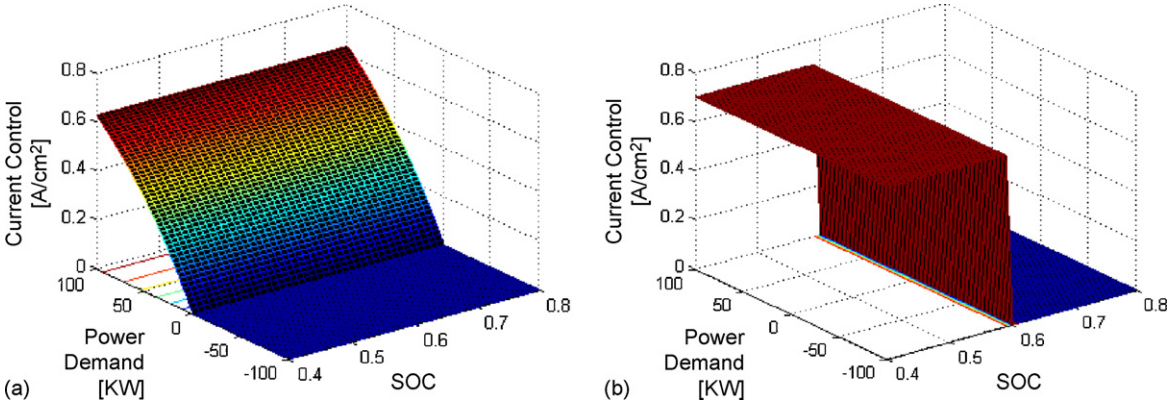

Fig. 13. Extreme cases of pseudo-SDP controller. The controller shape can vary flexibly such that it can generate from (a) "fuel cell only" controller, which operates mainly fuel cell system to follow vehicle power demand ($x_\alpha = 0, x_\sigma = 1$) to (b) "On/Off" controller, which switch the fuel cell system by battery SOC ($x_\alpha = \pi/2, x_\sigma = 100$).

Table 1
Comparison of Original SDP/Pseudo SDP control result

Driving Cycle		Original SDP controller	Pseudo SDP Controller		
			City cycle optimized	Highway cycle optimized	LA92 cycle optimized
City UDDS	MPGGE	**43.8**	**44.0**	43.4	43.7
	SOC bound (<0.2)	0.12	0.12	0.07	0.11
	max FCS rate (<12 KW/s)	12.2[a]	9.07	10.0	10.1
Highway HWFET	MPGGE	**43.9**	43.6	**43.9**	43.1
	SOC bound (<0.2)	0.09	0.17	0.07	0.14
	max FCS rate (<12 KW/s)	8.30	9.98	10.15	9.41
LA92	MPGGE	**34.6**	36.5	35.7	**35.9**
	SOC bound (<0.2)	0.26[a]	0.19	0.11	0.18
	max FCS rate (<12 KW/s)	11.5	13.3[a]	17.0[a]	11.5

[a] Failed to satisfy subsystem constraints.

to the SDP controller. Table 1 shows that the fuel economy results of the pseudo SDP controller are comparable to those of the original SDP controller. In this table, "MPGGE" stands for the miles per gallon gasoline equivalent (lower heating value basis), and "SOC bound" means the difference between maximum and minimum battery SOC during a driving cycle (lower "SOC bound" indicates more robustness in maintaining battery SOC upon vehicle power demand), and the maximum fuel cell system power rate in KW/s ("max FCS power rate") indicates the controller performance in protecting the fuel cell system from fast load change.

The fuel economy results achieved by the pseudo SDP controllers are comparable to that of the original SDP controller. In some cases, the pseudo SDP controller result is slightly better than that of the original SDP controller. This is because the pseudo SDP controller was optimized upon the specific driving cycle, while the original SDP controller was designed upon the averaged transition probability map. Although each pseudo SDP controller was optimized for a specific cycle, the performance of a pseudo SDP controller for other driving scenarios achieved good fuel economy as well. In other words, pseudo SDP control results are not cycle-beating.

Interesting results were found with the LA92 cycle, which is characterized by harder accelerations and higher speed than the UDDS city cycle. Except the LA92-cycle-optimized pseudo SDP controller, other three controllers failed to satisfy the subsystem constraint, either the SOC range limit or the fuel cell power rate limit. An advantage of the pseudo SDP controller over the original controller is that the parameters of the pseudo SDP controller can be modified easily to satisfy these subsystem constraints. Because the infinite horizon SDP controller only considers the probability transition map of a single time step, it does not have the capability to check the subsystem states over long period of time.

3.3. Optimization problem statement

We developed subsystem-scaling models and parameterized power management strategy, and they all can be included in the combined power management/design optimization problem statement as follows:

$$
\begin{aligned}
&\text{Minimize :} \quad f(\mathbf{x}) = (\text{fuel consumption}) \\
&\text{where } x = \{x_{i\max}, x_{\alpha}, x_{\sigma}, x_{\text{stableSOC}}, x_{\text{DOH}}, x_{\text{cp}}\} \\
&\qquad g_1(\mathbf{x}) = \frac{\max_k\{\text{SOC}(k)\}}{\text{SOC}^{\max}} - 1 \le 0 \\
&\qquad g_2(\mathbf{x}) = \frac{\text{SOC}^{\min}}{\min_k\{\text{SOC}(k)\}} - 1 \le 0 \\
&\text{subject to :} \quad g_3(\mathbf{x}) = \frac{|\text{SOC}(1) - \text{SOC}(N)|}{\Delta\text{SOC}^{\max}} - 1 \le 0 \\
&\qquad g_4(\mathbf{x}) = \frac{\max_k\{P_{\text{fcNet}}(k)\}}{P_{\text{fcNet}}^{\max}} - 1 \le 0 \\
&\qquad g_5(\mathbf{x}) = \frac{\max_k\{\Delta P_{\text{fcNet}}(k)\}}{\Delta P_{\text{fcNet}}^{\max}} - 1 \le 0
\end{aligned}
\tag{21}
$$

The first four design variables are assigned for the near-optimal controller, as explained in Section 3.1. The degree of hybridization x_{DOH} determines both the number of fuel cells and the battery capacity. Since the number of fuel cells is in the order of hundreds, so its value is assumed continuous. The battery SOC limit is given by the battery management system. As a conservative target, 0.5 and 0.7 are used for lower and upper bounds of SOC. The difference between initial and final SOC of time horizon (ΔSOC) is limited up to 1.5%. After each simulation, the fuel consumption is adjusted by ΔSOC assuming linear system charging efficiency. The FC net power during driving cycles is obtained from the non-causal FCS model. Last but not the least, we impose a limit for the changing rate of the FC power. The FCS model used in our study is static, and it does not capture dynamic

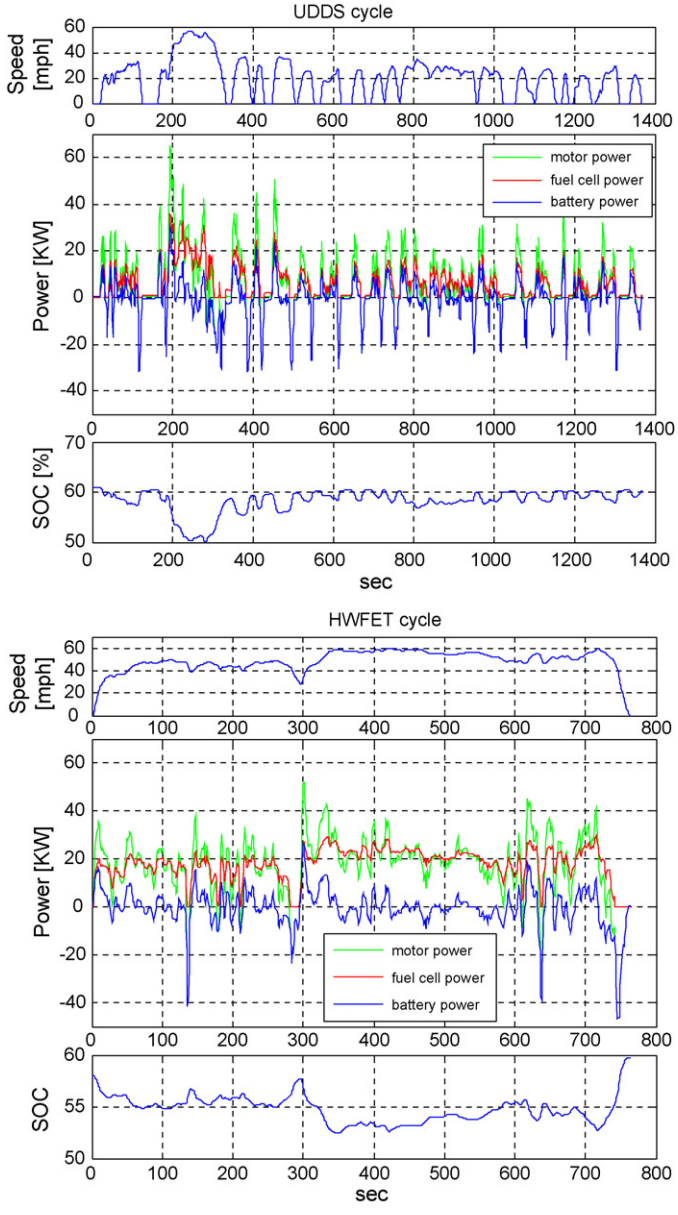

Fig. 14. Combined power management/design optimization result in time horizon of city (above)/highway (below) cycle. Overall, the fuel cell power range is mitigated by the battery while the battery SOC is maintained.

Table 2
Results of optimal design and constraints

	Units	Lower bound	Upper bound	UDDS city cycle		HWFET Highway cycle			ECE-EUDC
				Power management only	Power management/ design	Power management only	Power management/ design	Power management/ design[b]	Control/ Design
$x^*_{i\max}$	A/cm^2	0.1	2	0.525	0.525	0.521	0.525	0.521	0.525
x^*_{α}	rad	0	1.57	0.245	0.295	0.748	0.954	0.243	0.356
x^*_{α}	–	0	10	0.938	0.266	2.31	1.25	0.312	1.71
$x^*_{\text{stableSOC}}$	SOC	0.45	0.75	0.619	0.611	0.581	0.582	0.611	0.604
x^*_{DOH}	–	0.2	0.95	0.5[a]	0.654	0.5[a]	0.550	0.850	0.622
x^*_{cp}	–	0.5	1.5	1[a]	0.750	1[a]	0.866	0.732	0.867
g_1	max SOC			−0.097	−0.127	−0.149	−0.147	−0.08	−0.114
g_2	min SOC			−0.024	0	−0.048	−0.026	−0.086	0
g_3	ΔSOC			−0.027	−0.367	−0.002	−0.017	+0.99[b]	−0.001
g_4	max FCS power			−0.445	−0.011	−.433	−0.260	−0.173	−0.031
g_5	max FCS power rate			−0.051	0	0	0	0	−0.113
f^*	MPGGE			41.35	48.35	42.90	44.56	49.07	47.56

[a] Fixed parameters of the baseline design.
[b] ΔSOC constraint is moderated (−1.5% < ΔSOC < 3%).

problems such as oxygen starvation or compressor choke. Thus, the net power rate is limited to 12 kW s^{-1}, at which value the baseline design will reach its maximum net power within 5 s.

The objective function of this problem depends on nonlinear maps, which are somewhat noisy. It is difficult to use gradient-based optimization algorithms. Therefore, DIRECT algorithm [17] is used. DIRECT is a sampling algorithm, which can reduce possibility of converging to local minima in a noisy response surface.

4. Optimization results

Table 2 summarizes the optimization results in miles per gallon gasoline equivalent (MPGGE) for three driving cycles: FTP-72 (city), HWFET (highway), and ECE-EUDC. Here "power management only" optimization means that only the pseudo-SDP controller is optimized at fixed baseline component sizes whereas "power management and design" includes the optimization of component sizing in addition to the power management strategy. The "power management and design"

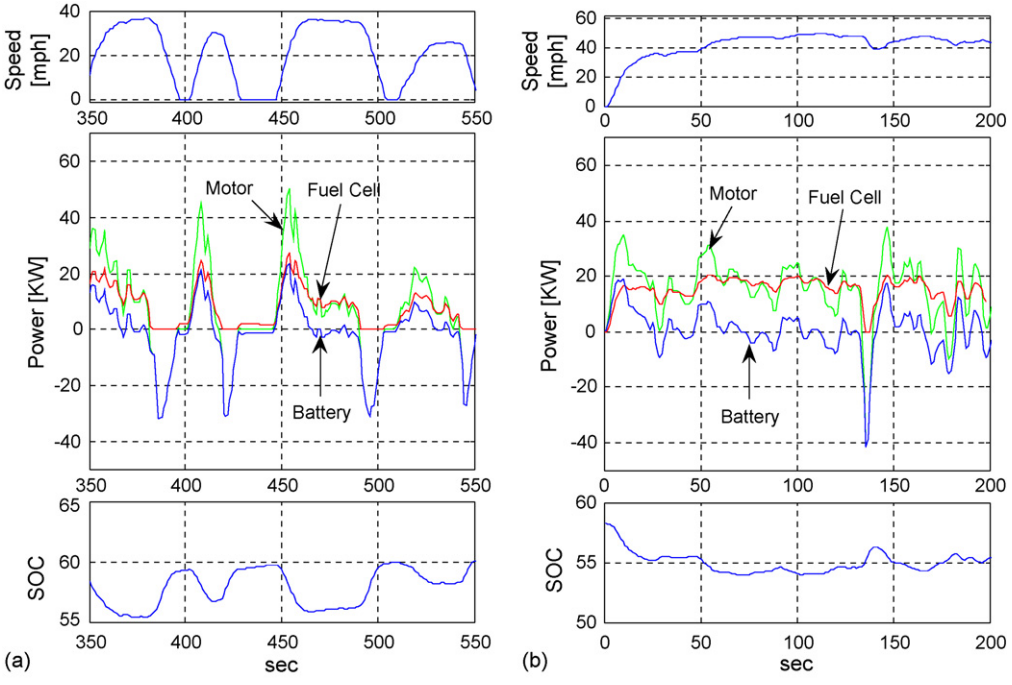

Fig. 15. Comparison of optimization results for 200 s of (a) city cycle (b) highway cycle.

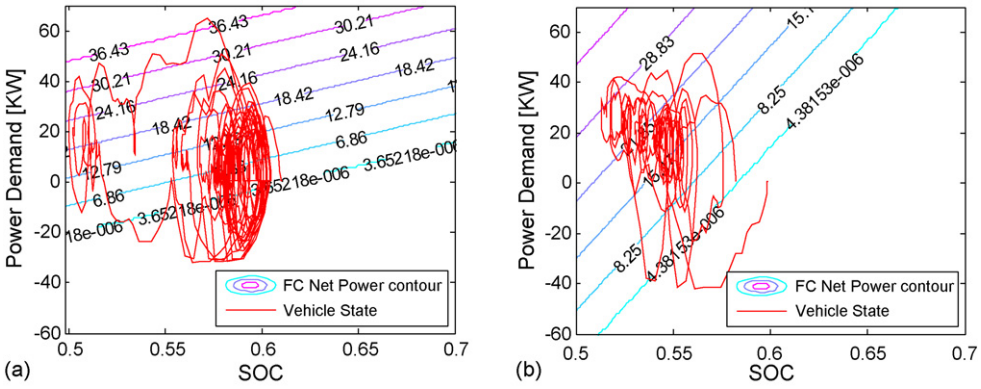

Fig. 16. Optimized controller map and vehicle state trajectories (a) city cycle (b) highway cycle. The optimal controller runs the fuel cell system mostly in the more efficient low power range. The city cycle generates more regenerative braking energy, so its SOC sensitivity slope of the controller is not as steep as that of the highway cycle.

optimization result shows 17% better fuel economy than the "power management only" optimization result for the city cycle. On the other hand, there was relatively small fuel economy improvement of 4% for the highway cycle. There is a hard deceleration at the end of the highway cycle, so the battery SOC increases significantly at the end. When the upper limit of ΔSOC constraint $g_3(x)$ was moderated from 1.5% to 3% for the highway cycle, 10% improvement of fuel economy (MPGGE: 49.07) could be achieved.

Unlike some strategies that depletes or overcharge the battery, our controller demonstrates that it can maintain the battery SOC within limited operating range. In Fig. 14, the optimization result in time horizon of city and highway cycles was shown. Similar to the original SDP controller, the pseudo-SDP controller split the required motor power to the fuel cell and the battery and maintains the battery SOC.

In Fig. 15, optimization results for city and highway cycles are compared. The city cycle of Fig. 15(a) has more accelerations/decelerations so the vehicle can capture more regenerative braking energy. Therefore, the optimized sensitivity slope of the city cycle is relatively flat compared to that of the highway cycle, i.e., $x^*_{\alpha,\text{city}} < x^*_{\alpha,\text{highway}}$ (Fig. 16). Fig. 15(b) shows the results for the first 200 s of highway cycle, in which the vehicle is launching and then cruising at 50 mph. When the vehicle first launched, the power demand suddenly increases and the battery helps to assist power for the FCS, of which the net power rate is limited. When the vehicle cruises, the pseudo-SDP controller runs the FCS "slow and steady" while the battery operates as an energy buffer to cover the fast dynamics of power demand.

The optimization process downsizes the compressor and increases the DOH. Thus, the FCS efficiency increases in the lower net power range from 0 to 25 kW, where the optimized FC engine primarily operates (Fig. 17). The maximum efficiency of the optimized FC engine is around 55% where that of the baseline design in Fig. 7 is around 50%. Although the downsized compressor here reduces the maximum net power of the FCS, the optimized pseudo-SDP controller successfully runs the FCS within the reduced maximum net power limit. Fig. 17(b) shows that even though the increased DOH reduces the battery size, the optimized battery design can still capture the majority of regenerative braking energy within its reduced power limit.

If fuel cell vehicles go into production in the near future, their degree of hybridization will significantly impact the vehicle price due to high manufacturing and material costs of fuel cells and batteries. Therefore, by examining the effect of DOH on fuel economy, car manufacturers can determine the trade-off between fuel savings and manufacturing costs. Fig. 18 illustrates the effect of the DOH on fuel economy for the city cycle. To

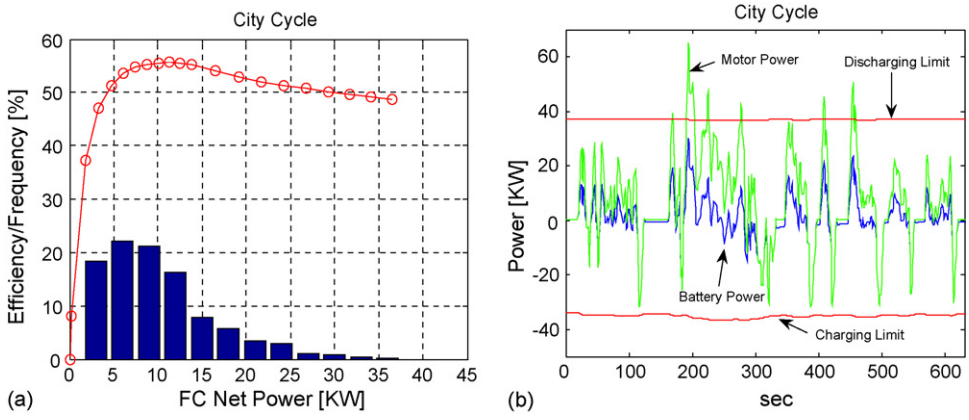

Fig. 17. Optimized (a) fuel cell and (b) battery characteristics for city cycle.

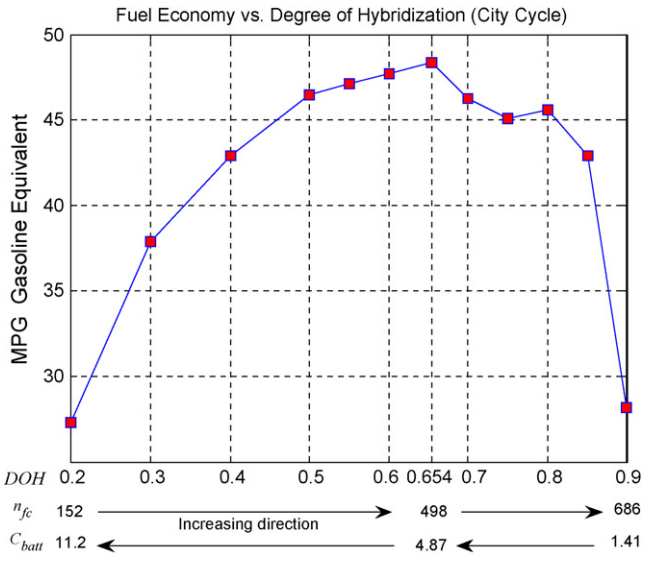

Fig. 18. Effect of degree of hybridization on fuel economy for city cycle.

obtain each point of the graph, the DOH value is first set, and then other five design variables are optimized to get the maximum fuel economy for the specific value of DOH. The results show that the optimal DOH is around 0.654. Compared to the baseline design, the number of fuel cells was increased from 381 to 498, whereas the battery capacity could be decreased from 7.035 to 4.87 Ah. As the DOH increases from 0.2 to 0.6, the fuel economy improves because the fuel cell efficiency increases. When the DOH goes beyond 0.75, the fuel economy drops because decreased battery capacity fails to capture the regenerative braking energy. Similar result was found by Toyota [7] although they did not describe if their power management strategy was optimized for each level of DOH.

5. Conclusions

We suggested a comprehensive and systematic framework that makes it possible to optimize power management and component sizing simultaneously for the future design of FCHVs. To achieve that, we essentially formulated a combined power management/design optimization problem of a FCHV. To reduce computational requirement of optimization process, we designed a near-optimal "pseudo-SDP controller". Unlike heuristic rule-based algorithms, this pseudo-SDP controller can generate near-optimal results due to its similarity to our optimal SDP controller. Because the pseudo-SDP controller can be represented with only a few variables, it can be therefore easily included as design variables in the optimization process. We also presented subsystem-scaling models that can predict the effect of sizing parameters on the system efficiency characteristics. Because the compressor size significantly influences the overall efficiency of a fuel cell system, we mainly focused on it for the fuel cell system-scaling model. The combined optimization results show that the optimality lies in: (1) downsizing the fuel cell compressor; (2) increasing degree of hybridization without compromising regenerative braking; (3) employing corresponding control strategy.

References

[1] Y. Guezennec, T.-Y. Choi, G. Paganelli, G. Rizzoni, Proceedings of the American Control Conference, Denver, CO, 2003.
[2] P. Rodatz, G. Paganelli, A. Sciarretta, L. Guzzella, Control Eng. Pract. 13 (2005) 41–53.
[3] A. Sciarretta, L. Guzzella, C.H. Onder, Automatisierungstechnik 51 (2003) 195–203.
[4] H. Fathy, J. Reyer, P. Papalambros, A. Ulsoy, Proceedings of the American Control Conference, Arlington, VA, 2001.
[5] D. Assanis, G. Delagrammatikas, R. Fellini, Z. Filipi, J. Liedtke, N. Michelena, P. Papalambros, D. Reyes, D. Rosenbaum, A. Sales, M. Sasena, Mech. Struct. Mach. 27 (4) (1999) 393–421.
[6] R. Fellini, N. Michelena, P. Papalambros, M. Sasena, Proceedings of the First International Symposium on Environmentally Conscious Design and Inverse Manufacturing, Tokyo, Japan, February 1–3, IEEE Comput. Soc, Los Alamitos, CA, 1999, pp. 400–405.
[7] T. Ishikawa, S. Hamaguchi, T. Shimizu, T. Yano, S. Sasaki, K. Kato, M. Ando, H. Yoshida, Development of next generation fuel-cell hybrid system—consideration of high voltage system, SAE Paper No. 2004-01-1304.
[8] P. Atwood, S. Gurski, D. Nelson, K. Wipke, T. Markel, Degree of hybridization modeling of a hydrogen fuel cell PNGV-class vehicle, SAE Paper No. 2002-01-1945.
[9] K. Wipke, T. Markel, D. Nelson, Proceedings of the 18th Electric Vehicle Symposium, Berlin, Germany, 2003.
[10] A. Rousseau, P. Sharer, R. Ahluwalia, Energy storage requirements for fuel cell vehicle, SAE Paper No. 2004-01-1302.
[11] T. Markel, M. Zolot, K.B. Wipke, A.A. Pesaran, Proceeding of Advanced Automotive Battery Conference, Nice, France, June, 2003.
[12] M.-J. Kim, H. Peng, C.-C. Lin, E. Stamos, D. Tran, Proceedings of the American Control Conference, Portland, OR, 2005.
[13] D.D. Boettner, G. Paganelli, Y.G. Guezennec, G. Rizzoni, M.J. Moran, ASME J. Energy Resour. Technol. 124 (1) (2002) 20–27.
[14] C.-C. Lin, M.-J. Kim, H. Peng, J. Grizzle, ASME J. Dyn. Syst. Meas. Control 128 (4) (2006) 878–890.
[15] J.P. Jensen, A.F. Kristensen, S.C. Sorenson, N. Houbak, E. Hendricks, Mean value modeling of a small turbocharged diesel engine, SAE910070.
[16] USDOE, FreedomCAR battery test manual for power-assist hybrid electric vehicles, DOE/ID-11069, Contract DE-AC07-99-ID13727, October 2003.
[17] D.R. Jones, C.D. Perttunen, B.E. Stuckman, J. Optimization Theory Appl. 79 (1) (1993) 157–181.